SEMARAK ILMU PUBLISHING

Journal of Advanced Research in Applied Sciences and Engineering Technology

Journal homepage:
https://semarakilmu.com.my/journals/index.php/applied_sciences_eng_tech/index
ISSN: 2462-1943

Generalized Mean-Based Joint Segmentation and Registration Model on High-Noise Multi-Modal Images

Nurul Asyiqin Mohd Fauzi[1], Mazlinda Ibrahim[2,*], Hoo Yann Seong[2], Abdul Kadir Jumaat[3,4], Lavdie Rada[5], Haider Ali[6]

[1] Pusat PERMATA@Pintar Negara, Universiti Kebangsaan Malaysia, 43600 Bangi, Selangor, Malaysia
[2] Department of Mathematics, Center for Defence Foundation Studies, National Defence University of Malaysia,57000 Kuala Lumpur, Malaysia
[3] School of Mathematical Sciences, College of Computing, Informatics and Media, Universiti Teknologi MARA (UiTM), 40450 Shah Alam, Selangor, Malaysia
[4] Institute for Big Data Analytics and Artificial Intelligence (IBDAAI), Universiti Teknologi MARA (UiTM), 40450 Shah Alam, Selangor, Malaysia
[5] Biomedical Engineering Department, Bahcesehir University, Besiktas, Istanbul, Turkey
[6] Department of Mathematics, University of Peshawar, Peshawar, Pakistan

ARTICLE INFO

Keywords:
Variational model; segmentation; registration; generalized mean; multi-modal images

ABSTRACT

Medical imaging plays a critical role in clinical decision-making and patient care. However, the presence of high levels of noise in medical images can significantly impact the accuracy of diagnosis and subsequent analysis. In recent years, joint segmentation and registration models have emerged as an effective alternative approach for enhancing medical images. Nevertheless, traditional methods, such as the Chan-Vese model, face challenges when dealing with images with high levels of noise. To address this limitation, this paper introduces a different approach that incorporates generalized mean into the joint model. Our joint model combines the generalized mean-based image segmentation which utilizes the fuzzy-membership function, modified normalized gradient fields and linear curvature for registration task. The performance of the proposed model is tested on 2D synthetic and real medical images with and without the presence of the white Gaussian noise. Then it is compared to the existing joint model using three evaluation criterions which are Dice coefficient metric, registration value and computational time. The proposed joint model improved by 60% according to the numerical results when tested on images with high level of noise. The model is useful and beneficial to the radiologists to perform quantitative analysis in assessing disease progression, response to treatment, and overall patient health.

1. Introduction

Medical imaging plays a crucial role in modern healthcare by enabling accurate diagnosis and treatment planning. However, the presence of noise in medical images poses a significant challenge to both clinicians and researchers. High-noise medical images hinder not only visual interpretation but also impede subsequent analysis and processing tasks. In recent years, various techniques have

* *Corresponding author.*
E-mail address: mazlinda@upnm.edu.my

https://doi.org/10.37934/araset.63.1.87102

been proposed to enhance such images. For instance, Ismail *et al.,* [1] developed a variational approach-based model for denoising and segmenting noisy images. However, achieving both noise reduction and preservation of vital anatomical details remains a formidable task. Meanwhile, joint segmentation and registration (JSR) models for medical images have shown remarkable potential by simultaneously addressing both tasks of segmenting anatomical structures and aligning images for accurate comparison and analysis.

There are numerous works related to JSR models, with many of them utilizing active contour based variational approaches. The models are based on active contour without edges, also known as the Chan-Vese (CV) model proposed by Chan and Vese [2]. Wali *et al.,* [3] considered the CV model to be one of the most successful classical models in variational image segmentation. The CV model has been a popular choice for image segmentation in JSR models. In 2011, Le Guyader and Vese [4] presented a combined matching criterion based on the CV model for topology preservation in segmentation task and incorporating the nonlinear elastic principle as the regularization term. This allowed for more significant deformation in their JSR model.

Ibrahim *et al.,* [5] improved upon the JSR model Le Guyader and Vese [4] by incorporating regularized Heaviside sum of the squared difference (SSDH) into the model and substituting the previous regularization term with the linear curvature model by Fischer and Modersitzki [6], resulting a smoother transformation. However, SSDH is only effective when the images have comparable intensities. Swierczynski *et al.,* [7] further proposed the merging of the CV model with active dense displacement field estimations based on level set formulation. Nevertheless, these variational methods mentioned only work with mono-modal images.

Mono-modal images are derived from a single imaging modality, such as magnetic resonance imaging (MRI), computed tomography (CT), or ultrasound whereas multi-modal images are created by combining data from different imaging modalities. This fusion of information enhances the diagnostic capabilities by offering a comprehensive view of the underlying anatomy and pathology such as PET-CT fusion combines positron emission tomography (PET) and CT scans to obtain metabolic information from PET along with precise anatomical localization from CT. It is useful for cancer staging, detecting metastases, and evaluating treatment response.

Significant advancements have been made in research to accommodate multi-modal images, as these images are more difficult to segment and register due to their different intensities as mentioned in Li *et al.,* [8]. For instance, Ademaj *et al.,* [9] used the CV segmentation model and improved the joint model by Ibrahim *et al.,* [5] with weighted Heaviside in mutual information (MI) into the JSR model for multi-modal images deformation. Ibrahim *et al.,* [10] further upgraded the joint model in Ademaj *et al.,* [9] by replacing weighted Heaviside MI (MIH) for the registration task with weighted Heaviside normalized gradient fields (NGFH), focusing on non-rigid multi-modal images. The joint model outperforms MIH in terms of JSR tasks when tested using the same medical images as Ademaj *et al.,* [9]. Additionally, Begum *et al.,* [11] developed a JSR model by using Bhattacharyya distance to deal with noise and intensity differences in multi-modal registration. Their JSR model also outperformed the JSR model in [9] when tested with a variety of noise levels.

Despite the advancements towards multi-modal images, these variational JSR models have a few limitations. Firstly, most of these JSR models are designed to improve registration task only. It was discovered that to enhance the registration task, the segmentation task must also be improved. This is because the segmentation provides an initial guess to help the registration task to transform the images in the JSR model as mentioned in Pawar *et al.,* [12]. Secondly, no further research or experiments have been conducted on noisy images. On top of that, the CV segmentation model is known to perform poorly on images with inhomogeneous intensities and the model is sensitive to high levels of noise as mentioned in Ali *et al.,* [13]. Furthermore, the minimization of CV model is non-

convex which can lead to local minima, which makes the optimization process challenging [14]. Therefore, the aim is to enhance the segmentation task in the JSR model and evaluate it on noisy multi-modal images.

In addition to the active contour models, a different approach in variational models can accommodate images with noise and outliers which is the fuzzy theory and logic based variational model [15]. Fuzzy logic is a mathematical framework that deals with uncertainty and imprecision in data. In image processing, fuzzy logic is used to handle and manipulate images based on their fuzzy or uncertain characteristics. The pixels in the images can belong to more than one group and set of membership level is associated with each pixel. Based on Alawad *et al*., [16], fuzzy logic is superior to other approaches because it accounts for the inherent lack of exactness in many situations, structuring its understanding to accommodate uncertainty. Krinidis and Chatzis [17] were the first to pioneer the integration of the fuzzy logic into the active contour framework. This novel fuzzy energy-based active contour can deal with objects with discontinuous or extremely smooth and undefined gradient boundaries. The fuzzy energy function acts as the model motivation power, evolving along the contour until it reaches the desired object boundary, which is determined by image color and spatial elements instead of the image gradient. This model is expressed in terms of a pseudo-level set function, where the active contour is represented by a particular value of the level set function known as the fuzzy membership function.

Wu *et al.,* [18] enhanced the prior work of Krinidis and Chatzis [17] by incorporating a kernel metric that can detect boundaries precisely and perform well with images in the presence of noise, outliers, and low contrast. Mondal *et al.,* [19] proposed a robust fuzzy energy based active contour that integrates information from both local and global energy terms. Local information which consists of the spatial distance and pixel intensity are used to cope with high intensity inhomogeneity and image noise, while global information is required to prevent undesirable outcomes due to poor initialization. Mondal [20] initiated a new multi-phase fuzzy energy based active contour model that emphasizes on multiple regions instead of two regions. It was inspired by Krinidis and Chatzis [17] with an upgraded version of the new multi-phase pseudo level set framework.

Rahman *et al.,* [21] and Ali *et al.,* [22] extended segmentation based fuzzy logic approach by using a fuzzy membership function and power mean. It is an effective segmentation model for images with multiple objects and various types of noise. Instead of a pseudo level set function, Rahman *et al.,* [21] used the fuzzy membership function to reject the local minima. The new power mean was developed to mitigate the negative effect of outliers. The proposed model in Rahman *et al.,* [21] produced superior segmentation results compared to other well-known fuzzy logic-based segmentation models when dealing with images with a high level of noise.

Inspired by Rahman *et al.,* [21] and Ali *et al.,* [22], the power mean or generalized mean (GM) for segmentation, along with NGFH and linear curvature for registration from Ibrahim *et al.,* [10], are integrated to enhance the performance of the JSR model with high-noise multi-modal images. To the best of our knowledge, this is the first time a fuzzy membership function approach has been implemented in the JSR framework that focuses on noisy multi-modal images. Before describing the model, the previous related work of the fuzzy-based JSR model is mentioned. El-Melegy and Mokhtar [23] initiated the integration of fuzzy framework into simultaneous segmentation and registration model. However, they used the prior information to segment the brain MRI into the fuzzy C-Mean algorithm. Here, the registration process was done using sum squared differences (SSD) which is only suitable for mono-modal applications. Then, El-Melegy *et al.,* [24] extended their work by embedding level set method into the FCM clustering for the dynamic contrast-enhanced magnetic resonance imaging (DCE-MRI) kidney datasets. Despite employing the level set method, the model in El-Melegy *et al.,* [24] consists of a shape prior model that must be trained for their registration to function

correctly. As is widely known, train models are limited and dependent on the datasets that are available, whereas no training is required by our model.

This paper focuses on the JSR model using the GM and fuzzy membership function-based segmentation model as well as NGFH with linear curvature as the regularization term for registration. The performance of the proposed JSR model is evaluated and compared with a variational JSR model that used the CV model and NGFH namely as the CV-NGFH model, initiated by Ibrahim *et al.,* [10] using the Dice coefficient metric, Reg_p and computational time. The images used in the evaluation are 2D multi-modal images comprising sets of synthetic and real multi-modal images from Ademaj *et al.,* [9] and Ibrahim *et al.,* [10] with additional white Gaussian noise. The proposed model which consists of the GM and the NGFH denoted as GM-NGFH outperformed the state-of art model when the images have high level of noise.

The structure of this paper is as follows: In the first section, an overview of the GM segmentation model and the CV-NGFH model is presented. Next, the proposed JSR model is introduced in the second section. In the third section, a comparison is made using three performance metrics on 2D real and synthetic medical images. Conclusions of this paper are described in the last section.

2. Methodology

2.1 Generalized Mean (GM) Model

Defined an image I on $\Omega \subset \Re^2$, and $\Omega_i \subseteq \Omega$ are disjoint connected open subsets with a piecewise smooth boundary C where $I(x) > 0$ is the intensity value at a certain pixel in which $x = (x_1, x_2)$. The minimization functional of GM is expressed as:

$$F(z(x), c_1, c_2) = \mu \int_\Omega |\nabla z(x)| dx + \int_\Omega w(x)|I(x) - c_1|^2 [z(x)]^2 dx + \int_\Omega y(x)|I(x) - c_2|^2 [1 - z(x)]^2 dx \quad (1)$$

where the fuzzy membership function, $z(x)$ are defined as follow:

$$\begin{aligned} &C = \{(x_1, x_2) \in \Omega : z(x) = 0.5\}, \\ &\text{inside } (C) = \{(x_1, x_2) \in \Omega : z(x) > 0.5\}, \\ &\text{outside } (C) = \{(x_1, x_2) \in \Omega : z(x) < 0.5\} \end{aligned} \quad (2)$$

along with,

$$w(x) = (|I(x) - c_1|^2)^{p-1}, \text{ and} \quad (3)$$

$$y(x) = (|I(x) - c_2|^2)^{p-1} \quad (4)$$

where p represents the power value in which $p \neq 0$. The parameter p controls the contribution of each sample's element by handling each of them differently according to their significance. It is selected based on the desired properties, such as sensitivity to outliers or robustness to noise. The values of c_1 and c_2, the inside and the outside of the C are updated through $w(x)$ and $y(x)$ in Eq. (3) and Eq. (4) for each step until it converges. The values of c_1 and c_2 are given by:

$$c_1 = \frac{\int_\Omega w(\boldsymbol{x}) \mathrm{I}(\boldsymbol{x}) [\mathrm{z}(\boldsymbol{x})]^p d\boldsymbol{x}}{\int_\Omega w(\boldsymbol{x}) [\mathrm{z}(\boldsymbol{x})]^p d\boldsymbol{x}}, \quad c_2 = \frac{\int_\Omega y(\boldsymbol{x})\, \mathrm{I}(\boldsymbol{x})\, [1 - \mathrm{z}(\boldsymbol{x})]^p d\boldsymbol{x}}{\int_\Omega y(\boldsymbol{x})\, [1 - \mathrm{z}(\boldsymbol{x})]^p d\boldsymbol{x}} \quad (5)$$

By keeping c_1 and c_2 fixed in Eq. (1), then minimized $F(\mathrm{z}(\boldsymbol{x}), c_1, c_2)$ with respect to z and $\mu = 0$, it becomes:

$$z = \frac{1}{1+\left(\frac{w(x)|I(x)-c_1|^2}{y(x)|(x)-c_2|^2}\right)} \tag{6}$$

Based on Rahman *et al.,* [21], the updated value of $\mathrm{z}(x)$ is used in the Euler-Lagrange equation obtained by minimized $F(\mathrm{z}(x), c_1, c_2)$ with respect to z and $\mu \neq 0$. The Euler-Lagrange equation is solved by introducing τ as an artificial time and using fully explicit scheme. The GM segmentation model framework is summarized in Table 1.

Table 1
Algorithm 1: GM segmentation model framework

BEGIN
Input: Image, $\boldsymbol{I}(\boldsymbol{x})$
Output: The segmentation of image, $\boldsymbol{z}(\boldsymbol{x})$

1. Initialization:
$$\boldsymbol{I}, \boldsymbol{p}, \boldsymbol{\mu}, \boldsymbol{maxit}$$
2. For $\boldsymbol{iter} = \mathbf{1}, \ldots\ldots, \boldsymbol{maxit}$
   (a) Update $\boldsymbol{w}(\boldsymbol{x})$ and $\boldsymbol{y}(\boldsymbol{x})$ using Eq. (3) and Eq. (4).
   (b) Update the value of $\boldsymbol{c_1}$ and $\boldsymbol{c_2}$ using Eq. (5).
   (c) Update $\mathbf{z}(\boldsymbol{x})$ using Eq. (6).
   (d) Update $\mathbf{z}(\boldsymbol{x})$ using explicit scheme (refer to equation 39 in Rahman *et al.*, [21].)
3. End For.
4. Compute the segmentation of the image $\boldsymbol{I}$ using $\boldsymbol{z}(\boldsymbol{x})$.

END

2.2 Chan-Vese and Modified Normalized Gradient Fields (CV-NGFH)

Ibrahim *et al.,* [10] incorporates the CV model as their segmentation model, NGFH and linear curvature as regularization term concentrating on non-rigid multi-modal registration. In their JSR model, the authors modified NGF by Haber and Modersitzki [25] and incorporating regularized Heaviside function which becomes the CV-NGFH model. Let the template image denotes as *T* and the reference image as *R*. Ibrahim *et al.,* [10] aim to match the template image and segment the reference image to demonstrate the deformation of the displacement field lead by the segmentation task. The joint model applied the CV model as their segmentation model to segment *T* to produce the zero-level set, $\phi_0(x)$. The image *T* is a bounded function, and it is formed by two regions that are separated by a curve or contour Γ. Let Γ represent the region of the object where the intensity of *T* is approximated by the value c_1 for the inside Γ whereas the value c_2 for the outside Γ. The segmentation of *T* is represented by zero level set of a Lipschitz function $\phi_0 \colon \Omega \to \mathbb{R}$ to represent target contour Γ such that,

$$\begin{cases} \Gamma = \partial\Omega_1 = \{(x_1, x_2) \in \Omega \mid \phi(x_1, x_2) = 0\} \\ \text{inside } (\Gamma) = \Omega_1 = \{(x_1, x_2) \in \Omega \mid \phi(x_1, x_2) > 0\} \\ \text{outside } (\Gamma) = \Omega_2 = \{(x_1, x_2) \in \Omega \mid \phi(x_1, x_2) < 0\} \end{cases} \tag{7}$$

Hence, the CV model minimizes the following variational formulation problem as:

$$\min_{c_1,c_2,\Gamma} F^{CV}(\phi(x),c_1,c_2) = \mu \int_\Omega \delta\big(\phi(x)\big)|\nabla\phi(x)|dx + \omega_1 \int_\Omega (T(x)-c_1)^2 H(\phi(x))dx + \omega_2 \int_\Omega (T(x)-c_2)^2(1-H(\phi(x)))dx \quad (8)$$

where the first term penalized the length. It should be mentioned that, according to Saibin *et al.,* [26], the first term is also known as the total variation term. Saibin *et al.,* [26] highlighted that using the Gaussian kernel is faster in computing time for regularizing the level set function compared to the total variation term. The second and third terms in Eq. (8) penalized discrepancy between the piecewise constant model and template image, T. The $\mu \geq 0$, $\omega_1, \omega_2 > 0$ are fixed parameters. *H* is the Heaviside function and δ is the Dirac delta function. To compute the Euler-Lagrange equation, both *H* and δ functions shall be regularized since *H* is not differentiable at 0. Both regularized functions denoted as:

$$H_\varepsilon(x) = \frac{1}{2}\left(1 + \frac{2}{\pi}\arctan\left(\frac{x}{\varepsilon}\right)\right), \delta_\varepsilon(x) = H'_\varepsilon(x) = \frac{\varepsilon}{\pi(\varepsilon^2+x^2)} \quad (9)$$

As $\varepsilon \longrightarrow 0$, both approximations are converged to *H* and δ. Hence, the regularized functional of Eq. (8) is given by:

$$\min_{c_1,c_2,\Gamma} F_\varepsilon^{CV}(\phi(x),c_1,c_2) = \mu \int_\Omega \delta_\varepsilon\big(\phi(x)\big)|\nabla\phi(x)|dx + \omega_1 \int_\Omega (T(x)-c_1)^2 H_\varepsilon(\phi(x))dx + \omega_2 \int_\Omega (T(x)-c_2)^2(1-H_\varepsilon(\phi(x)))dx \quad (10)$$

By letting $\phi(x)$ fixed and minimize Eq. (10) with respect to $c_{1,}c_2$, we have,

$$c_1 = \frac{\int_\Omega T(x)H_\varepsilon(\phi(x))dx}{\int_\Omega H_\varepsilon(\phi(x))dx}, c_2 = \frac{\int_\Omega T(x)(1-H_\varepsilon(\phi(x)))dx}{\int_\Omega (1-H_\varepsilon(\phi(x)))dx} \quad (11)$$

where the values of $c_1$and c_2 represent the average intensity inside and outside the boundary $\phi_0(\boldsymbol{x})$ in the reference image. Then, the Euler Lagrange equation for ϕ is given by:

$$\mu\delta_\varepsilon\big(\phi(x)\big)\nabla\cdot\left(\frac{\nabla\phi(x)}{|\nabla\phi(x)|}\right) - \omega_1\delta_\varepsilon\big(\phi(x)\big)(T(x)-c_1)^2 + \omega_2\delta_\varepsilon(\phi(x))(T(x)-c_2)^2 = 0,$$
$$\frac{\partial\phi(x)}{\partial\vec{n}} = 0 \quad (12)$$

In variational image registration, the transformation is formulated as $\rho(x) = x + u(x)$, where $\rho(x)$ is the transformation vector. The transformation allows us to find the displacement vector field, $u(x) = \big(u_1(x), u_2(x)\big)$ with $x = (x_1, x_2)$. The joint functional proposed by Ibrahim *et al*., [10] is given as follows:

$$\min_{c_1,c_2,u(x)} \mathcal{J}(c_1,c_2,u(x)) = \lambda_1 \int_\Omega |R(x)-c_1|^2 H_\varepsilon\left(\phi_0\big(x+u(x)\big)\right)\mathrm{d}x + \lambda_2 \int_\Omega |R(x)-c_2|^2\left(1-H_\varepsilon\left(\phi_0\big(x+u(x)\big)\right)\right)\mathrm{d}x + \lambda_3 D^{\mathrm{NGFH}}(T,R,\phi_0(x),u(x)) + \alpha\mathcal{S}^{\mathrm{LC}}(u(x)) \quad (13)$$

where λ_1, λ_2, λ_3 are numerical constants, $u(x)$ is the displacement vector field, ϕ_0 is the zero level set and $\mathcal{D}^{\mathrm{NGFH}}$ is the modified NGF. By adopting level set formulation, $\phi_0(x)$ as in the CV model, Eq. (13) is minimize with respect to $c_1$and c_2, we obtain:

$$c_1 = \frac{\int_\Omega R(x) H_\varepsilon\big(\phi_0(x+u(x))\big)\mathrm{d}x}{\int_\Omega H_\varepsilon\big(\phi_0(x+u(x))\big)\mathrm{d}x}, c_2 = \frac{\int_\Omega R(x)\big(1-H_\varepsilon(\phi_0(x+u(x)))\big)dx}{\int_\Omega 1-H_\varepsilon(\phi_0(x+u(x)))dx} \tag{14}$$

Given by the NGF functional as follows:

$$\mathcal{D}^{\mathrm{NGF}}(T,R,u(x)) = \int_\Omega 1-(nT(x+u(x))^{\mathrm{T}} nR(x))^2 \mathrm{d}x \tag{15}$$

where,

$$nT(x+u(x)) = \frac{|\nabla T(x+u(x))|}{\sqrt{|\nabla T(x+u(x))|^2+\eta^2}} \tag{16}$$

for the template image and similarly for the reference image. This measure calculates the gradient of the images. The constant parameter η in Eq. (16) is essential as it determines the edges. It also represents modality dependence and aims for noise filteration. Then, Ibrahim *et al.,* [10] modified the NGF in Eq. (15) with the regularized Heaviside function, H_ε (Eq. (17)) to obtain Eq. (18) and the term $\mathcal{S}^{\mathrm{LC}}(u(x))$ in Eq. (13) is the linear curvature regularization term.

$$H_\varepsilon(\phi_0(x+u(x))) = \frac{1}{2}\left(1+\frac{2}{\pi}\arctan\frac{\phi_0(x+u(x))}{\varepsilon}\right) \tag{17}$$

$$\mathcal{D}^{\mathrm{NGFH}}\big(T,R,\phi_0(x),u(x)\big) = \int_\Omega [1-(nT(x+u(x))^T nR(x))^2] H_\varepsilon(\phi_0(x+u(x)))dx \tag{18}$$

$$\mathcal{S}^{\mathrm{LC}}(u(x)) = \int_\Omega \big(\Delta u_1(x)\big)^2 + \big(\Delta u_2(x)\big)^2 \mathrm{d}x \tag{19}$$

2.3 The Proposed Model: GM-NGFH

A variational JSR framework is proposed by combining the segmentation and registration to form joint functional $J(T,R,u(x),z(x))$. This framework is inspired by the two previously presented models. The proposed JSR model based on the GM model for segmentation and NGFH and linear curvature for registration namely the GM-NGFH model as the following functionals:

$$\begin{aligned}\min_{c_1,c_2,u(x)} J(c_1,c_2,u(x))\& = \mu\int_\Omega |\nabla z(x)|dx + \int_\Omega w(x)|R(x)-c_1|^2[z\big(x+u(x)\big)]^2 dx + \\ \int_\Omega y(x)|R(x)-c_2|^2[1-z\big(x+u(x)\big)]^2 dx + \\ \lambda_3 D^{NGFH}\big(T,R,z(x),u(x)\big) + \alpha\mathcal{S}^{LC}(u(x))\end{aligned} \tag{20}$$

where,

$$\mathcal{D}^{\mathrm{NGFH}}\big(T,R,z(x),u(x)\big) = \int_\Omega [1-(nT(x+u(x))^T nR(x))^2] H_\varepsilon(z(x+u(x)))dx \tag{21}$$

$\mathcal{S}^{\mathrm{LC}}(u(x))$ is given in Eq. (19), *T* and *R* refers to the template and reference images respectively. Meanwhile, $z(x)$ indicates as the segmentation of template image and $u(x)$ is the displacement vector field. To update $u(x)$, the functional in Eq. (20) is solved through optimization techniques. The Quasi-Newton method based on the Limited-memory Broyden–Fletcher–Goldfarb–Shanno (LBFGS) algorithm is used in a multilevel framework for faster implementation. The implementation for the proposed JSR model is then summarized in Table 2.

Table 2
GM-NGFH model framework

BEGIN
Input: Reference image, *R* and template image, *T*
Output: The transformed template image, $\boldsymbol{T}(\boldsymbol{x}+\boldsymbol{u}(\boldsymbol{x}))$ and segmentation of the reference image, $\boldsymbol{z}(\boldsymbol{x}+\boldsymbol{u}(\boldsymbol{x}))$

1. Initialization:
$$\boldsymbol{\alpha}, \boldsymbol{p}, \boldsymbol{\mu}, \boldsymbol{dt}, \boldsymbol{maxit}, \boldsymbol{\lambda_3}, \boldsymbol{minlevel}, \boldsymbol{maxlevel}, \boldsymbol{u}^{\boldsymbol{minlevel}} = \boldsymbol{0}$$
2. Segmentation of the template image using GM segmentation model to produce $\boldsymbol{z}(\boldsymbol{x})$. Please refer to Algorithm 1.
3. Coarsen *R, T,* $\boldsymbol{z}(\boldsymbol{x})$ to produce $\boldsymbol{T}^{\boldsymbol{level}}, \boldsymbol{R}^{\boldsymbol{level}}$ and $\mathbf{z}\ (\boldsymbol{x})^{\boldsymbol{level}}$ using standard coarsening method.
4. For *level = minlevel: maxlevel*
   (a) $\left(\boldsymbol{u}(\boldsymbol{x})^{\boldsymbol{level}},\ \boldsymbol{c_1},\ \boldsymbol{c_2}\right) \leftarrow$ LBFGS $\boldsymbol{J}\left(\boldsymbol{T}, \boldsymbol{R}, \mathbf{z}\ (\boldsymbol{x})^{\boldsymbol{level}}, \boldsymbol{u}(\boldsymbol{x})^{\boldsymbol{level}}, \boldsymbol{\lambda_1},\ \boldsymbol{\lambda_2}, \boldsymbol{\lambda_3}, \boldsymbol{\alpha}\ \right)$.

Please refer to LBFGS from Modersitzki [27].

   (b) If *level < maxlevel*, interpolate $\mathbf{z}\ (\boldsymbol{x})^{\boldsymbol{level}}$ and $\boldsymbol{u}(\boldsymbol{x})^{\boldsymbol{level}}$ to the next finer level (level = level +1) using linear interpolation.
5. End For.
6. Compute the transformed template image: $\boldsymbol{T}(\boldsymbol{x}+\boldsymbol{u}(\boldsymbol{x}))$ and the segmentation of the reference image $\boldsymbol{z}(\boldsymbol{x}+\boldsymbol{u}(\boldsymbol{x}))$.

END

3. Numerical Results

In this section, five experiments are performed on 2D synthetic multi-modal images of size 128 × 128. From the five experiments: Experiment 1 involves synthetic images while Experiment 2,3,4 and 5 involve real medical images. It is conducted by using MATLAB R2020b software with MATLAB Image Processing Toolbox on Windows 10. The CPU processor used was Intel® Core ™ i7-6700 CPU @ 3.40GHz with 16G RAM. For all experiments, the white Gaussian noise is added on the template images. The white Gaussian noise is a statistical noise that occurs frequently on most cases of images. It is generated by applying the random Gaussian function to the image function with zero mean.

The performance of our proposed model, the GM-NGFH model and the CV-NGFH model from Ibrahim *et al.,* [10] are evaluated and compared in the presence of the white Gaussian noise on five sets of 2D multi-modal real and synthetic medical images from Ademaj *et al.,* [9] and Ibrahim *et al.,* [10]. The three performance measures are the Dice coefficient metric, the registration performance measure, Reg_p and the computing time (in seconds). Additional performance metrics for image quality assessment, such as normalized absolute error, average difference, and misclassification, can be applied to compare models' performance [28].

The Dice coefficient metric is used to assess the segmentation accuracy, which evaluates the spatial overlap between the segmentation of the reference and the transformed template images. Meanwhile, the Reg_p is calculated to show the quality of the registration. For the computational time, we used the MATLAB tic toc functions to measure the elapsed time for each task performed. The formula of Dice coefficient metric to test the segmentation performance:

$$\text{Dice } (\%) = \frac{2|\text{Seg } (T(x+u(x)))\cap\text{Seg } (R(x))|}{|\text{Seg } (T(x+u(x)))|+|\text{Seg } (R(x))|} \times 100 \tag{22}$$

where $\text{Seg } (T(x+u(x)))$ is the segmentation of the transformed template image and $\text{Seg } (R(x))$ is the segmentation of the reference image. This coefficient is a good indicator for estimating the overlapping regions between the segmented image and the transformed template image. The segmented transformed template image matches closely to the reference image as the Dice value approaches 100%. Following is the registration performance measure, the Reg_p:

$$Reg_p = |\mathcal{D}^{MI}\left(T\left(x + u(x)\right), R(x)\right)| \tag{23}$$

where,

$$\mathcal{D}^{MI} = \int_{\Omega} \rho_{[T(x+u(x))]} \log \rho_{[T(x+u(x))]} dt + \int_{\Omega} \rho_{[R(x)]} \log \rho_{[R(x)]} dr - \int_{\Omega^2} \rho_{[T(x+u(x)),R(x)]} \log \rho_{[T(x+u(x)),R(x)]} d(t,r) \tag{24}$$

The $\rho_{[T(x+u(x))]}$ and $\rho_{[R(x)]}$ represent the probability distributions of pixel intensities for the transformed template image and the reference image, respectively whereas $\rho_{[T(x+u(x)),R(x)]}$ is the joint intensities distribution of both images. The range is $0 \leq Reg_p < \infty$ which signifies the values of mutual information between the transformed template image and reference image. The greater the value of Reg_p, the more accurate the registration task performed on those images. To determine the superior model, we also calculate the relative Dice and Reg_p. The relative formulas are calculated as follows:

$$Relative\ Dice\ (\%) = \left|\frac{Average\ Dice\ Model\ A - Average\ Dice\ Model\ B}{Average\ Dice\ Model\ A}\right| \times 100, \text{ and} \tag{25}$$

$$Relative\ Reg_p\ \ (\%) = \left|\frac{Average\ Reg_p\ Model\ A - Average\ Reg_p\ Model\ B}{Average\ Reg_p\ Model\ A}\right| \times 100 \tag{26}$$

On five sets of 2D real and synthetic multi-modal images of size 128 × 128 from Ademaj *et al.,* [9] and Ibrahim *et al.,* [10], the performance of segmentation models CV-NGFH and the GM-NGFH models are measured with varied noise intensities of white Gaussian noise. This experiment employs the Dice coefficient metric, the registration performance, Reg_p and the computational time. In this experiment, distinct noise levels are selected. The performance of each multi-modal image set is evaluated separately. N1 represents a low noise level, N2 represents a medium noise level, and N3 represents a high noise level. The different levels of noise are due to the variety of multi-modal images with varying intensities. In accordance with each set of 2D multi modal images, the experiment is divided into five separate experiments: Experiment MU1, Experiment MU2, Experiment MU3, Experiment MU4 and Experiment MU5. Figure 1 demonstrates the examples of the inputs and outputs for low-noise MU1 in the JSR tasks.

The GM model is implemented to segment the template image in Figure 1(a), in which the segmentation of the template image represents the initial level set in Figure 1(c). The red curves represent the segmentation contour. The segmentation of the template image is then incorporated into the JSR algorithm. Here, the level set is updated from the coarsest level to the finest level, while the transformation of the template image can be observed through the grid as shown in Figure 1(d). It is deformed until it reaches the finest level to produce the registered template image in Figure 1(e).

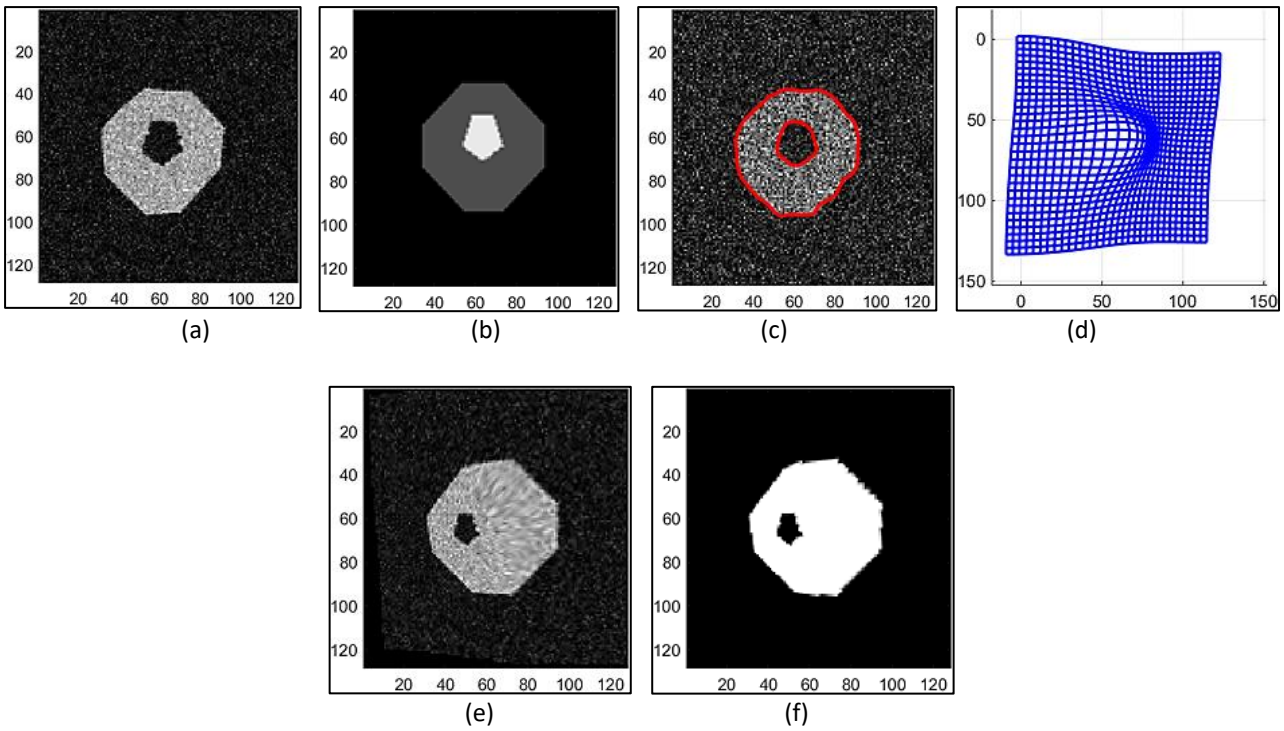

Fig. 1. Illustration of the input and outputs for low-noise MU1 (a) *N*oisy template image, *T* (b) *R*eference image, R (c) Segmentation of template image, $\phi_0(x)$ (d) Transformation, $u(x)$ (c) Transformed template image, $T\left(x+u(x)\right)$ (f) segmentation of template image, $\phi_0\left(x+u(x)\right)$

3.1 Experiment MU1: A Set of 2D Synthetic Noisy Images

In this experiment, the CV-NGFH and the GM-NGFH models are evaluated in the presence of the white Gaussian noise on 2D synthetic noisy images. The synthetic images are taken from Ademaj *et al.,* [9]. Figure 2 displays the reference and the template images with three different noise levels at N1 = 0.01, N2 = 0.05 and N3 = 0.1. Table 3 measures the performance of both JSR models by comparing the results of the Dice, Reg_p and the computing time at three different noise levels.

The results in Table 3 reveals that the GM-NGFH model yields a slightly higher Dice value for N1 by 0.11%. In contrast, the CV-NGFH model exceeded the GM-NGFH model by 0.33% and 0.02% for N2 and N3 respectively. Due to very small differences between both models, their segmentation accuracy in the presence of low to high noise levels are nearly equivalent. Moreover, the registration accuracy of the CV-NGFH model in N1, N2 and N3 are superior to the GM-NGFH model at 40.13×10^{-2}, 33.46×10^{-2} and 23.60×10^{-2} accordingly. The computing time for both models is comparable and less than sixty seconds. The results allowed us to conclude that the CV-NGFH model provides a more accurate representation of this noisy synthetic images.

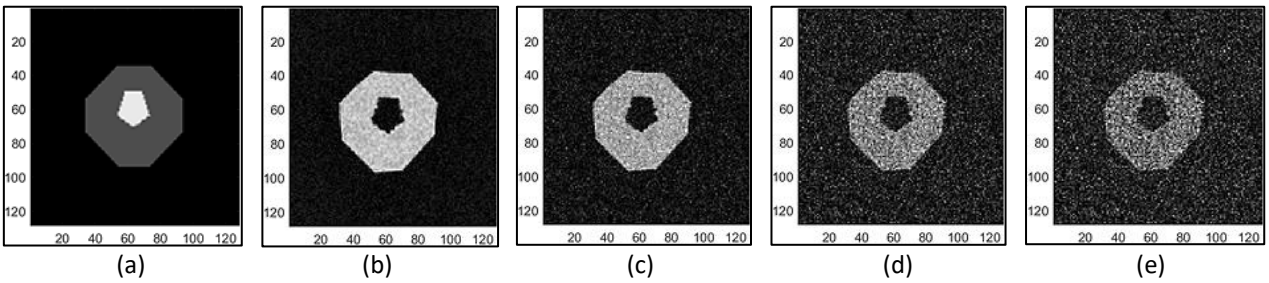

Fig. 2. (a) Reference synthetic image (b) Original template synthetic image (c) Template synthetic image with low noise level (N1) (d) Medium noise level (N2) (e) High level (N3)

Table 3
Comparison values of Dice, Reg_p and computational time for 2D noisy synthetic Image

Measure	N1		N2		N3	
	CV-NGFH	GM-NGFH	CV-NGFH	GM-NGFH	CV-NGFH	GM-NGFH
Dice (%)	84.64	84.75	65.39	65.06	56.96	56.94
$\boldsymbol{Reg_p}(\times \mathbf{10^{-2}})$	40.13	37.71	33.46	32.61	23.60	23.20
Computational time (s)	54.11	43.79	43.47	46.28	50.34	40.66

3.2 Experiment MU2: A Set of 2D T2-PD Brain MRIs

In this experiment, the 2D T2-PD brain MRIs from Ademaj *et al.,* [9] are used with the CV-NGFH and the GM-NGFH models. Figure 3 illustrated the brain MRIs with additional three noise levels of the white Gaussian noise where N1 = 0.005, N2 = 0.01 and N3 = 0.06. Table 4 compared the results of Dice, Reg_p and the computational time (in seconds) at three different noise levels.

Based on Table 4, the GM-NGFH model delivers slightly higher segmentation accuracy at 93.12%, 90.87% and 72.16% for N1, N2 and N3 respectively. Observably, the CV-NGFH model failed to segment the brain MRI at a noise level of 0.06. In addition, the registration quality of the CV-NGFH model in N1 and N2 is better than the GM-NGFH model by a difference of 1.01% and 0.99% accordingly. The GM-NGFH model had the quickest computation time and required the least amount of time to compute regardless of noise levels. Thus, the GM-NGFH is a suitable JSR model for these brain MRIs.

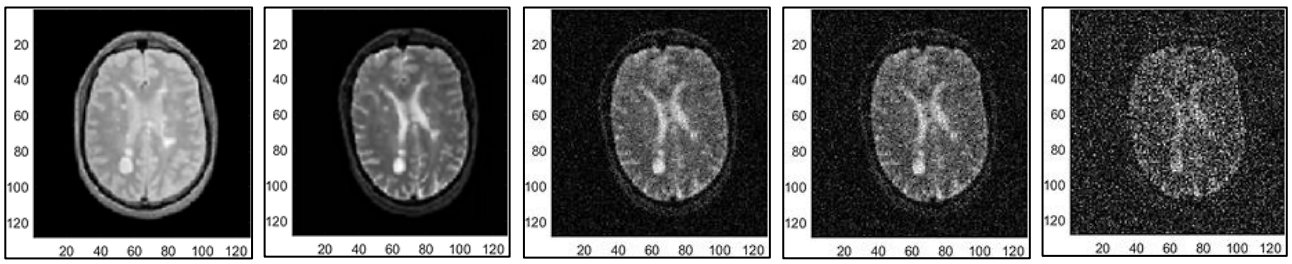

(a) (b) (c) (d) (e)

Fig. 3. Images for experiment MU2: A Set of 2D T2-PD Brain MRIs (a) Reference brain MRI (b) Original template image without noise (c) Template brain MRI with low level of the white Gaussian noise (d) Medium level noise (e) High level of noise

Table 4
The Dice, Reg_p and computational time for 2D noisy T2-PD brain MRIs

Measure	N1		N2		N3	
	CV-NGFH	GM-NGFH	CV-NGFH	GM-NGFH	CV-NGFH	GM-NGFH
Dice (%)	93.10	93.12	90.82	90.87	-	72.16
$\boldsymbol{Reg_p}(\times \mathbf{10^{-2}})$	60.30	59.69	55.56	55.01	-	22.21
Computational time (s)	58.29	47.66	60.43	43.04	-	42.75

3.3 Experiment MU3: A Set of 2D T1-T2 Brain MRIs

Both JSR models, the GM-NGFH and the CV-NGFH models are evaluated on 2D T1-T2 brain MRIs from Ibrahim *et al.,* [10] with the presence of the white Gaussian noise. Three noise levels of template, original template image and reference images are illustrated in Figure 4. The performance evaluation of the JSR models on noisy brain MRIs is presented in Table 5. The noise levels of the white Gaussian Noise are 0.015, 0.03 and 0.07.

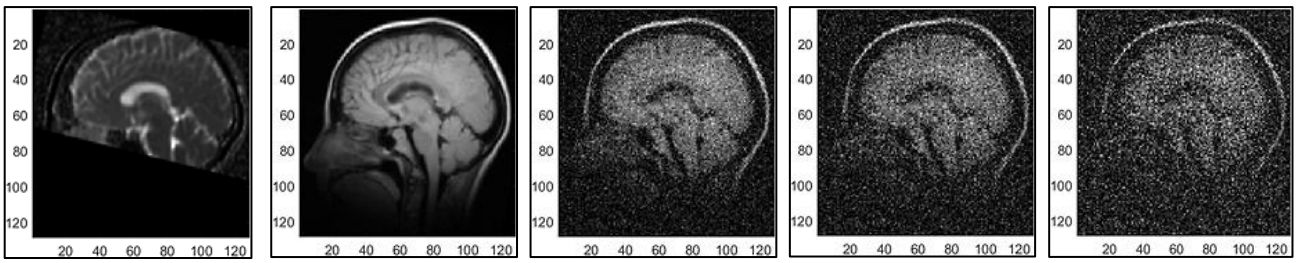

(a) (b) (c) (d) (e)

Fig. 4. The reference brain MRI in Experiment 3 (b) Template brain MRI without noise (c) Template brain MRI with low level (d) Template brain MRI with medium level of noise (e) Template brain MRI with high level of noise

Table 5
The Dice, Reg_p and computational time for 2D noisy T1-T2 brain MRIs

Measure	N1		N2		N3	
	CV-NGFH	GM-NGFH	CV-NGFH	GM-NGFH	CV-NGFH	GM-NGFH
Dice (%)	81.22	80.23	76.89	76.21	-	67.14
$\boldsymbol{Reg_p}(\times \mathbf{10^{-2}})$	33.45	32.43	26.67	25.55	-	14.37
Computational time (s)	39.08	39.40	38.02	39.30	-	42.38

In accordance with Table 5, the CV-NGFH model yields superior Dice values at 81.22%, 76.89% with a difference of 0.99% and 0.68% for N1 and N2. Same goes for the values of Reg_p, the CV-NGFH model outperforms the GM-NGFH model at 33.45×10^{-2} and 26.67×10^{-2}. Table 5 shows that the CV-NGFH model is incapable of generating values for noise levels of 0.07. This gives the GM-NGFH model an advantage as it can produce results at noise level of 0.07. In terms of computing time, both models have similar computational time of approximately 35s to 45s. Thus, the GM-NGFH model is a superior model for this set of multi-modal images.

3.4 Experiment MU4: A Set of 2D Brain MRIs

Experiment MU4 measured the CV-NGFH and the GM-NGFH models using brain MRIs acquired from Ibrahim *et al.,* [10]. Figure 5 shows three noise levels of template and reference brain MRIs used for Experiment MU4 in which N1 = 0.01, N2 = 0.05 and N3 = 0.1. The results of Dice, Reg_p and the computational time (in seconds) at three distinct noise levels are compared in Table 6.

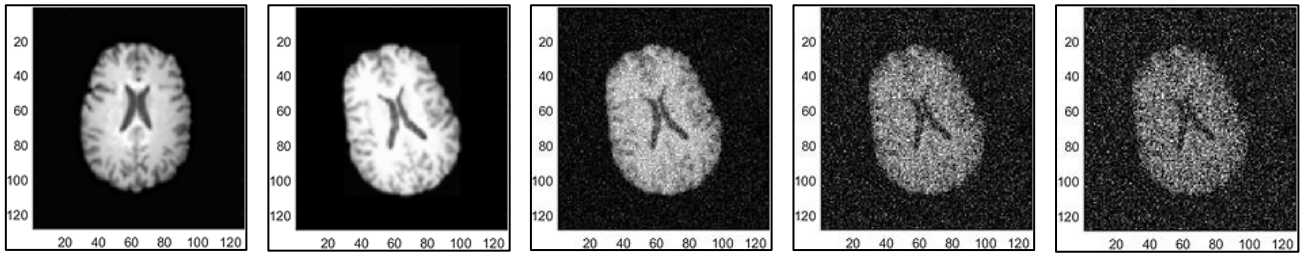

(a) (b) (c) (d) (e)

Fig. 5. Experiment MU4: A set of 2D Brain MRIs. (a) Reference brain MRI (b) Original template image without noise (c) Template brain MRI with low noise level (d) Medium noise level (e) High noise level

Based on Table 6, the CV-NGFH model produces more accurate segmentation based on the Dice values of N1 and N2 than the GM-NGFH model at 97.37% and 88.20% respectively. However, in N3, the GM-NGFH model performs slightly superior at 78.85%. In terms of Reg_p values, the GM-NGFH

model outperforms on all noise levels for N1, N2 and N3. The relative for Reg_p in N1, N2 and N3 are 1.8%, 0.75% and 4.86%. Meanwhile, the relative Dice in N1, N2 and N3 are 0.08%, 0.22% and 0.33% respectively. Therefore, it can be concluded that the GM-NGFH model provides superior segmentation and registration accuracy than the CV-NGFH model in the presence of low and high levels of noise.

Table 6
Result of Dice, Reg_p and computational time for 2D noisy brain MRIs

Measure	N1		N2		N3	
	CV-NGFH	GM-NGFH	CV-NGFH	GM-NGFH	CV-NGFH	GM-NGFH
Dice (%)	97.37	97.29	88.20	88.01	78.59	78.85
$\boldsymbol{Reg_p}(\times \mathbf{10^{-2}})$	63.09	64.24	51.98	52.37	38.29	40.15
Computational time (s)	55.55	90.38	76.31	84.51	1152.52	134.85

3.5 Experiment MU5: A Set of 2D T1-T2 Chest MRIs

Experiment MU5 assessed the CV-JSR models in the presence of white Gaussian noise using a set of 2D T1-T2 chest MRI images from Ademaj *et al.,* [9]. Figure 6 depicts the MU2 images of a reference image, template images without noise and with three noise levels that are applied to this experiment in which N1 = 0.01, N2 = 0.05 and N3 = 0.1. Table 7 compares the performance of the CV-NGFH and GM-NGFH models based the results of Dice, Reg_p and the computational time (in seconds) in three different noise levels.

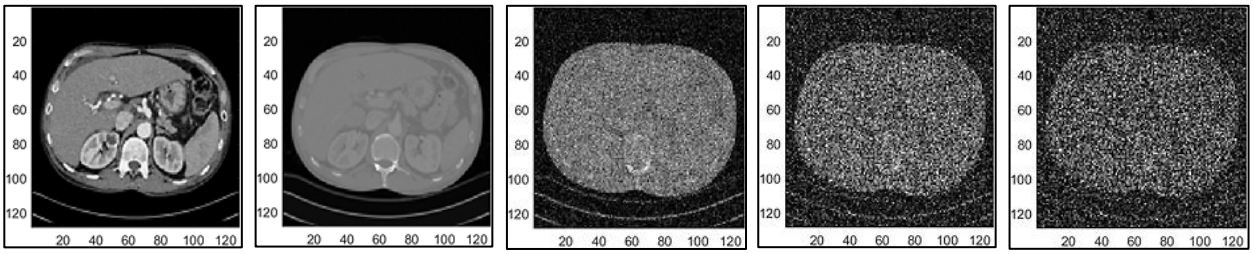

Fig. 6. (a) Reference chest MRI in Experiment 5 (b) Template chest MRI without noise (c) Template chest MRI with low level (d) Template chest MRI with medium level of noise (e) Template chest MRI with high level of noise

Table 7
The Dice, Reg_p and computational time for 2D noisy chest MRIs

Measure	N1		N2		N3	
	CV-NGFH	GM-NGFH	CV-NGFH	GM-NGFH	CV-NGFH	GM-NGFH
Dice (%)	90.25	90.16	79.00	80.44	70.22	-
$\boldsymbol{Reg_p}(\times \mathbf{10^{-2}})$	53.36	53.23	31.51	34.95	19.71	-
Computational time (s)	262.36	52.69	100.94	64.64	48.97	-

The Dice value of the CV-NGFH model is better at 90.25% compared to the GM-NGFH model at 90.16% in N1, as shown in Table 7. Nevertheless, in N2, the GM-NGFH model is superior by a margin of 1.44% over the CV-NGFH model. The relative Dice between the two models are 0.1% for N1 and 1.82% for N2. Meanwhile, the value of Reg_p in the CV-NGFH is 53.36×10^{-2} compared to 53.23×10^{-2} in the GM-NGFH model for N1. In N2, the GM-NGFH outperformed at 34.95×10^{-2}. The relative Reg_p in N1 and N2 are 0.24% and 10.92% for the CV-NGFH and GM-NGFH models respectively. In terms of computational time, the GM-NGFH model is the fastest compared to the CV-

NGFH model, at 52.69s and 64.64s for N1 and N2. Yet, the GM-NGFH model is incapable of generating results for a high noise level, N3. Therefore, we concluded that the CV-NGFH model is an ideal model for noisy chest MRIs.

4. Conclusions

Image segmentation and image registration are two essential steps in medical imaging. Despite their interrelationship, both tasks are often performed separately. Due to that, it faces several challenges and problems when undertaken independently. For example, the detection of false boundaries and inaccurate registration between medical images when there is a presence of noise. Therefore, the main objective of this study is to enhance the existing work of the JSR model in the presence of noise. This study proposes the GM-NGFH model, a new modified JSR model from the existing work of Ibrahim *et al.,* [10] by replacing the previous segmentation model, the CV model with a different segmentation model, namely the GM model.

In conclusion, both the CV-NGFH and the GM-NGFH models are suitable JSR models for noisy medical images. For mono-modal images, both models performed well at noise levels as high as 0.1. However, there are some cases, particularly in multi-modal images with the presence of the noise where the CV-NGFH model was unable to yield any results for specific noise levels especially those greater than 0.05. Meanwhile, the GM-NGFH produces good segmentation and registration results and improved by 60% when tested on multi-modal images with a high noise level. In addition, the GM-NGFH model could compute faster and require less amount of time to complete the JSR tasks in comparison to the CV-NGFH model. Therefore, the proposed model, the GM-NGFH model improves the CV-NGFH model in terms of accuracy and speed of JSR tasks in the presence of a high level of white Gaussian noise.

Conflict of interest

All authors are requested to disclose any actual or potential conflict of interest including any financial, personal or other relationships with other people or organizations within three years of beginning the submitted work that could inappropriately influence, or be perceived to influence, their work.

Acknowledgement

The research and writing of this work are funded by Ministry of Higher Education of Malaysia and National Defence University of Malaysia under grants RACER/1/2019/ICT01/UPNM/1 and UPNM/2022/GPPP/SG/15.

References

[1] Ismail, Nurhuda, Abdul Kadir Jumaat, and Nurul Fatin Azara Zulkarnain. "An improved variational-based model for denoising and segmentation of vector-valued images." *Journal of Advanced Research in Applied Sciences and Engineering Technology* 40, no. 1 (2024): 189-203. https://doi.org/10.37934/araset.40.1.189203

[2] Chan, Tony, and Luminita Vese. "An active contour model without edges." In International conference on scale-space theories in computer vision, p. 141-151. Berlin, Heidelberg: Springer Berlin Heidelberg, 1999. https://doi.org/10.1007/3-540-48236-9_13

[3] Wali, Samad, Chunming Li, Mudassar Imran, Abdul Shakoor, and Abdul Basit. "Level-set evolution for medical image segmentation with alternating direction method of multipliers." *Signal Processing* 211 (2023): 109105. https://doi.org/10.1016/j.sigpro.2023.109105

[4] Le Guyader, Carole, and Luminita A. Vese. "A combined segmentation and registration framework with a nonlinear elasticity smoother." *Computer Vision and Image Understanding* 115, no. 12 (2011): 1689-1709. https://doi.org/10.1016/j.cviu.2011.05.009

[5] Ibrahim, Mazlinda, Ke Chen, and Lavdie Rada. "An improved model for joint segmentation and registration based on linear curvature smoother." *Journal of Algorithms & Computational Technology* 10, no. 4 (2016): 314-324. https://doi.org/10.1177/1748301816668027

[6] Fischer, Bernd, and Jan Modersitzki. "A unified approach to fast image registration and a new curvature based registration technique." *Linear Algebra and Its Applications* 380 (2004): 107-124. https://doi.org/10.1016/j.laa.2003.10.021

[7] Swierczynski, Piotr, Bartłomiej W. Papież, Julia A. Schnabel, and Colin Macdonald. "A level-set approach to joint image segmentation and registration with application to CT lung imaging." *Computerized Medical Imaging and Graphics* 65 (2018): 58-68. https://doi.org/10.1016/j.compmedimag.2017.06.003

[8] Li, Lei, Wangbin Ding, Liqin Huang, Xiahai Zhuang, and Vicente Grau. "Multi-modality cardiac image computing: A survey." *Medical Image Analysis* 88 (2023): 102869. https://doi.org/10.1016/j.media.2023.102869

[9] Ademaj, Adela, Lavdie Rada, Mazlinda Ibrahim, and Ke Chen. "A variational joint segmentation and registration framework for multimodal images." *Journal of Algorithms & Computational Technology* 14 (2020): 1748302620966691. https://doi.org/10.1177/1748302620966691

[10] Ibrahim, Mazlinda, Lavdie Rada, Adela Ademaj, and Ke Chen. "Non-rigid joint segmentation and registration using variational approach for multi-modal images." In *Progress in Intelligent Decision Science*: *Proceeding of IDS 2020*, p. 99-112. Springer International Publishing, 2021. https://doi.org/10.1007/978-3-030-66501-2_8

[11] Begum, Nasra, Noor Badshah, Lavdie Rada, Adela Ademaj, Muniba Ashfaq, and Hadia Atta. "An improved multi-modal joint segmentation and registration model based on Bhattacharyya distance measure." *Alexandria Engineering Journal* 61, no. 12 (2022): 12353-12365. https://doi.org/10.1016/j.aej.2022.06.018

[12] Pawar, Aishwarya, Yongjie Jessica Zhang, Cosmin Anitescu, and Timon Rabczuk. "Joint image segmentation and registration based on a dynamic level set approach using truncated hierarchical B-splines." *Computers & Mathematics with Applications* 78, no. 10 (2019): 3250-3267. https://doi.org/10.1016/j.camwa.2019.04.026

[13] Ali, Haider, Lavdie Rada, and Noor Badshah. "Image segmentation for intensity inhomogeneity in presence of high noise." IEEE Transactions on Image Processing 27, no. 8 (2018): 3729-3738. https://doi.org/10.1109/TIP.2018.2825101

[14] Brown, Ethan S., Tony F. Chan, and Xavier Bresson. "Completely convex formulation of the Chan-Vese image segmentation model." International journal of computer vision 98 (2012): 103-121. https://doi.org/10.1007/s11263-011-0499-y

[15] Saibin, Tammie Christy, Abdul Kadir bin Jumaat, and Marina Yusoff. "Variational fuzzy energy active contour models for image segmentation: A review." In *2023 4th International Conference on Artificial Intelligence and Data Sciences (AiDAS)*, p. 293-297. IEEE, 2023. https://doi.org/10.1109/AiDAS60501.2023.10284601

[16] Alawad, Abdulrahman Moffaq, Farah Diyana Abdul Rahman, Othman O. Khalifa, and Norun Abdul Malek. "Fuzzy logic based edge detection method for image processing." *International Journal of Electrical and Computer Engineering* 8, no. 3 (2018): 1863. https://doi.org/10.11591/ijece.v8i3.pp1863-1869

[17] Krinidis, Stelios, and Vassilios Chatzis. "Fuzzy energy-based active contours." *IEEE Transactions on Image Processing* 18, no. 12 (2009): 2747-2755. https://doi.org/10.1109/tip.2009.2030468

[18] Wu, Yue, Wenping Ma, Maoguo Gong, Hao Li, and Licheng Jiao. "Novel fuzzy active contour model with kernel metric for image segmentation." *Applied Soft Computing* 34 (2015): 301-311. https://doi.org/10.1016/j.asoc.2015.04.058

[19] Mondal, Ajoy, K. Ramachandra Murthy, Ashish Ghosh, and Susmita Ghosh. "Robust image segmentation using global and local fuzzy energy based active contour." In *2016 IEEE international conference on fuzzy systems (FUZZ-IEEE),* p. 1341-1348. IEEE, 2016. https://doi.org/10.1109/FUZZ-IEEE.2016.7737845

[20] Mondal, Ajoy. "Fuzzy energy based active contour model for multi-region image segmentation." Multimedia tools and applications 79 (2020): 1535-1554. https://doi.org/10.1007/s11042-019-08207-7

[21] Rahman, Afzal, Haider Ali, Noor Badshah, Muhammad Zakarya, Hameed Hussain, Izaz Ur Rahman, Aftab Ahmed, and Muhammad Haleem. "Power mean based image segmentation in the presence of noise." *Scientific Reports* 12, no. 1 (2022): 21177. https://doi.org/10.1038/s41598-022-25250-x

[22] Ali, Haider, Amna Shujjahuddin, and Lavdie Rada. "A new active contours image segmentation model driven by generalized mean with outlier restoration achievements." International Journal of Pattern Recognition and Artificial Intelligence 34, no. 11 (2020): 2054026. https://doi.org/10.1142/S0218001420540269

[23] El-Melegy, Moumen, Rasha Kamel, Mohamed Abou El-Ghar, Norah S. Alghamdi, and Ayman El-Baz. "Variational approach for joint kidney segmentation and registration from DCE-MRI *Using Fuzzy Clustering with Shape Prior*s." *Biomedicines* 11, no. 1 (2022): 6. https://doi.org/10.3390/biomedicines11010006

[24] El-Melegy, Moumen, and Hashim Mokhtar. "Fuzzy framework for joint segmentation and registration of brain MRI with prior information." In *The 2010 International Conference on Computer Engineering & Systems*, p. 9-14. IEEE, 2010. https://doi.org/10.1109/icces.2010.5674904

[25] Haber, Eldad, and Jan Modersitzki. "Intensity gradient based registration and fusion of multi-modal images." In *Medical Image Computing and Computer-Assisted Intervention–MICCAI 2006: 9th International Conference, Copenhagen, Denmark, October 1-6, 2006. Proceedings, Part II 9*, p. 726-733. Springer Berlin Heidelberg, 2006. https://doi.org/10.1007/11866763_89

[26] Saibin, Tammie Christy, and Abdul Kadir Jumaat. "Variational selective segmentation model for intensity inhomogeneous image." *Indonesian Journal of Electrical Engineering and Computer Science* 29, no. 1 (2023): 277-285. https://doi.org/10.11591/ijeecs.v29.i1.pp277-285

[27] Modersitzki, Jan. *FAIR: flexible algorithms for image registration*. Society for Industrial and Applied Mathematics, 2009. https://doi.org/10.1137/1.9780898718843

[28] Mustafa, Wan Azani, Haniza Yazid, Mastura Jaafar, Mustaffa Zainal, Aimi Salihah Abdul-Nasir, and Noratikah Mazlan. "A review of image quality assessment (iqa): Snr, gcf, ad, nae, psnr, me." *Journal of Advanced Research in Computing and Applications* 7, no. 1 (2017): 1-7.